

# High Energy Electron Generation by Laser-Cone Interaction

Tatsufumi NAKAMURA, Hitoshi SAKAGAMI<sup>1)</sup>, Tomoyuki JOHZAKI, Hideo NAGATOMO, Kunioki MIMA and James KOGA<sup>2)</sup>

*Institute of Laser Engineering, Osaka University, Suita 565-0871, Japan*

<sup>1)</sup>*Theory and Computer Simulation Center, National Institute for Fusion Sciences, Toki 509-5292, Japan*

<sup>2)</sup>*Kansai Photon Science Institute, Japan Atomic Energy Agency, Kyoto 619-0215, Japan*

(Received 16 February 2007 / Accepted 17 April 2007)

Electron acceleration processes taking place in the interaction of ultra-intense laser pulses with cone targets are studied by using two-dimensional Particle-in-Cell (PIC) simulations to understand the characteristics of electrons generated from cone targets. It is explained that there are two dominant acceleration processes which are distinctive in the laser-cone interaction. One is the acceleration and transport along the side wall of the cone target, where electrons are guided along the side wall surface towards the cone tip by surface magnetic and electric fields. The second is the ponderomotive acceleration at the cone tip by the laser field which is intensified by cone focusing. The understanding of these acceleration processes helps to design cone targets to control the electron energy characteristics.

© 2007 The Japan Society of Plasma Science and Nuclear Fusion Research

Keywords: laser-cone interaction, surface acceleration, ponderomotive force, proton acceleration

DOI: 10.1585/pfr.2.018

## 1. Introduction

Recent progress in laser technology has opened up new research fields in high energy density physics, such as X-ray generation with high brightness, charged particle acceleration with high quality [1–3], fast ignition research in inertial fusion [4], and so on. In the fast ignition scheme, cone targets are used to guide the heating laser pulse close to the core plasma which is surrounded by a large-scale corona plasma, and to generate high energy charged particles which heat up the core plasma. Advantages in using cone targets were verified in experiments, which show a huge increase in the neutron yield by using cone targets [5]. But much of the physics is not clearly understood yet, and are now being intensively studied experimentally and numerically [6, 7]. One of the key issues is the generation of high energy particles from the cone target. It is shown by 3D Particle-in-cell (PIC) simulation that cone targets focus laser energy and high energy electrons at the cone tip which result in higher coupling efficiency from the laser to electrons [8]. In this paper, we investigate the interaction between intense laser pulses and cone targets by using 2D PIC simulation in order to clarify the electron acceleration and transport processes to understand the characteristics of electrons generated in the laser-cone interaction. Understanding this is quite important in designing the optimum cone shape for fast ignition, and determining the basis for using cone targets as devices for generating high energy charged particles [9].

This paper is organized as follows. In Sec. 2, we show comparisons of electron characteristics generated from a

cone target and a plane target which are irradiated by intense laser pulses to show the advantages of cone targets. In Sec. 3, two dominant electron acceleration processes taking place in the laser-cone interaction are explained. The effective temperature for electrons generated at the cone wall is reduced from the ponderomotive energy of the incident laser pulse, and that for the electrons generated at the cone tip is enhanced. In Sec. 4, proton acceleration by the laser-cone interaction is shown as one application of electron energy control by the cone target. Summary and conclusions are given in Sec. 5.

## 2. Comparison Between a Cone and Plane Geometry Target

Cone targets have advantages in the generation of high energy electrons when irradiated by ultra-intense laser pulses, such as the high energy absorption rate and the potential to control electron energy characteristics. In order to show the distinctive features of cone targets, electron energy spectra from cone and plane targets are compared. The simulation conditions are as follows. The initial density profile of the cone target is shown in Fig. 1 (a). The target density is 100 times the critical density which is defined as  $n_c = m\epsilon_0\omega_0^2/e^2$  where  $m$  and  $e$  are electron mass and charge,  $\epsilon_0$  and  $\omega_0$  are the dielectric constant in vacuum and the laser frequency, respectively. Preplasmas exist on the inner side of the cone target which have exponential profiles whose scale lengths are  $1.0\mu\text{m}$  and  $0.27\mu\text{m}$  at the cone tip and cone side wall, respectively. An overdense plasma which models the corona plasma surround-

author's e-mail: nakamura@ile.osaka-u.ac.jp

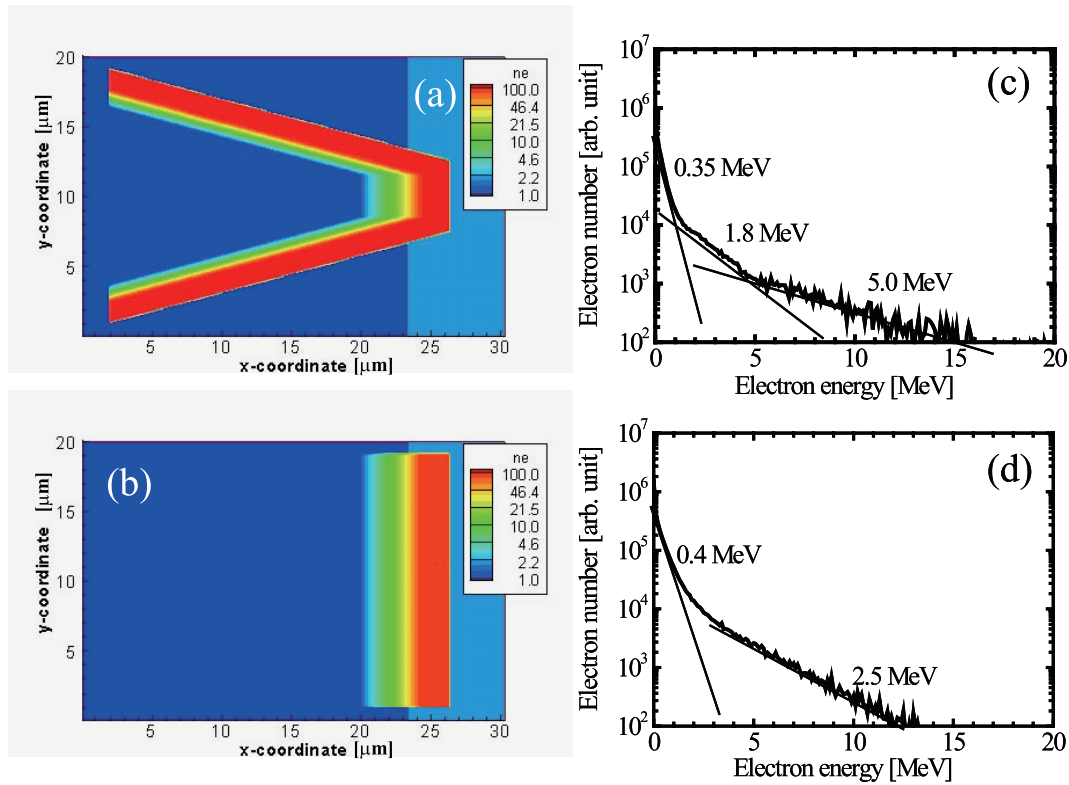


Fig. 1 Initial profile of the cone target and plane target are shown in (a) and (b). Electron spectra observed from the rear side of the (c) cone target and (d) plane target, which are irradiated by intense laser pulses of  $1.5 \times 10^{19}$  W/cm<sup>2</sup> and 150 fs.

ing the core is located at the rear side of the cone target whose density is  $2 n_c$ . The initial electron temperature is 10 keV, and ions are kept immobile. Laser pulses irradiate the target from the left boundary whose irradiance is  $5.0 \times 10^{19}$  W/cm<sup>2</sup> with 1.0  $\mu$ m wavelength, which corresponds to a normalized vector potential which is defined by  $a_0 = \sqrt{I [\text{W/cm}^2] \lambda_L^2 [\mu\text{m}^2] / 1.4 \times 10^{18}}$  of 6.0. The laser field is linearly polarized in the  $y$ -direction with a Gaussian profile whose spot size is 10  $\mu$ m (FWHM). The laser pulse rises up in 5 laser cycles and sustains its peak intensity for 150 fs. A plane target is used for comparison, which is modeled as a flattened cone geometry keeping other parameters constant, i.e., the target maximum density is 100  $n_c$  with a preplasma of 1.0  $\mu$ m scale length, and surrounded by a  $2 n_c$  plasma on the rear side, as shown in Fig. 1 (b). The laser conditions are exactly same as those used in the cone simulation. The diffraction effect due to the propagation to plane target is negligible, since the Rayleigh length of the laser pulse is much larger than the distance to the target.

In Figs. 1 (c) and 1 (d), time-integrated electron energy spectra observed 2  $\mu$ m behind the targets are plotted. In the plane target case, the electron spectrum is fitted by Maxwellian distributions with two temperatures. The lower temperature is 0.4 MeV for electrons in the energy range of  $\leq 2.0$  MeV. The higher temperature is 2.5 MeV, which is well approximated by the ponderomotive energy

which is expressed as [10]

$$T_h = mc^2 \left( \sqrt{1 + a_0^2} - 1 \right). \quad (1)$$

The electron spectrum from the cone target shown in Fig. 1 (c) is fitted by Maxwellian distributions with three temperatures. The lowest temperature is  $T_{\text{low}} \approx 0.35$  MeV which is almost same as in the plane case. But the other two temperatures differ from the ponderomotive energy of the incident laser pulse. The electrons whose energy  $E$  is  $2.0 \leq E [\text{MeV}] \leq 5.0$  are fitted with  $T_{\text{mid}} \approx 1.9$  MeV, and the electrons with higher energy are fitted with  $T_{\text{high}} \approx 5.0$  MeV which is much higher than the ponderomotive energy of the incident lasers. The results having an additional slope temperature indicates that there are two dominant acceleration processes taking place in laser-cone interaction.

In the plane target irradiation, the energy characteristics of the high energy electrons are simply determined by the incident laser irradiance. But in the cone target case, the electron energy can be modified from energy estimated from the incident laser irradiance. This indicates that cone targets have the possibility to control the electron energy characteristics by changing the cone geometry without changing the laser irradiance, which is an advantage of the cone targets. Another advantage of the cone target is the higher energy absorption rate. A laser pulse irradiates the target surface more than once for the cone target case due to the multiple reflections inside the target,

which results in a higher energy absorption rate. Because the cone targets have additional parameters such as cone angle and scale length at the side wall compared to plane targets, it is difficult to derive a general quantity as to how much the absorption rate increases. But in the above simulations the absorption rate of the cone target is twice as high as that of the plane target.

### 3. Electron Acceleration Processes

An important feature of the laser-cone interaction is having a large interaction region at the cone wing, where the laser irradiates the target with a relatively large incident angle and its irradiance on the surface becomes lower than at  $90^\circ$  irradiation as is plane target irradiation. As the cone open angle becomes smaller maintaining the diameters of the cone entrance and tip, the interaction region becomes larger and the laser fields irradiate the side wall at larger incident angle. In the case of a  $30^\circ$  cone target, the laser field interacts with the target side wall with an incident angle of  $75^\circ$ . In this case, high energy electrons are effectively transported along the target surface with a static surface magnetic field [8, 11]. In Fig. 2 (a) the longitudinal component of the current distribution  $J_x$  is plotted. From the figure it is seen that high energy electrons flow in the underdense region, more precisely, the effective underdense region with  $n_e \leq \gamma n_c$  where  $\gamma$  is the Lorentz factor, and the return current flows just inside the critical surface to sustain current-neutrality. As a result, a huge magnetic field which is about 200 Mega Gauss is induced along the surface, as is shown in Fig. 2 (b). Surface transport is also seen in the intense laser irradiation at a plane target with large incident angle [11]. When the intense laser pulse irradiates a target with a sharp density gradient, electrons are pushed towards the laser wave vector, which results in current filament formation via magnetic field instability. In the case of a large incident angle such as  $75^\circ$ , some electrons flow in the lateral direction which smooths out the surface non-uniformity of alternating layers of forward and backward current filaments, and form a surface current layer and magnetic field which are aligned along the target surface. Surface magnetic field prevents high energy electrons from penetrating into the target, and guides them along the surface toward the tip with the aid of surface sheath field. The effective temperature for electrons accelerated at cone wing is fitted by  $T_{\text{mid}}$  (see also Fig. 3 (b) where  $T_{\text{mid}}$  is measured at  $x = 10$ ), which does not strongly depend on the coordinate.  $T_{\text{mid}}$  is lower than the ponderomotive energy of incident laser pulse which is 2.5 MeV in the above condition, and higher than the ponderomotive energy calculated by taking into account the intensity decrease due to oblique irradiation, whose tendency is seen in targets of different cone angle with similar size. When the surface potential and laser electric field co-exist, electrons are effectively accelerated along the surface by wiggling inside the potential [12, 13]. When the surface acceleration takes

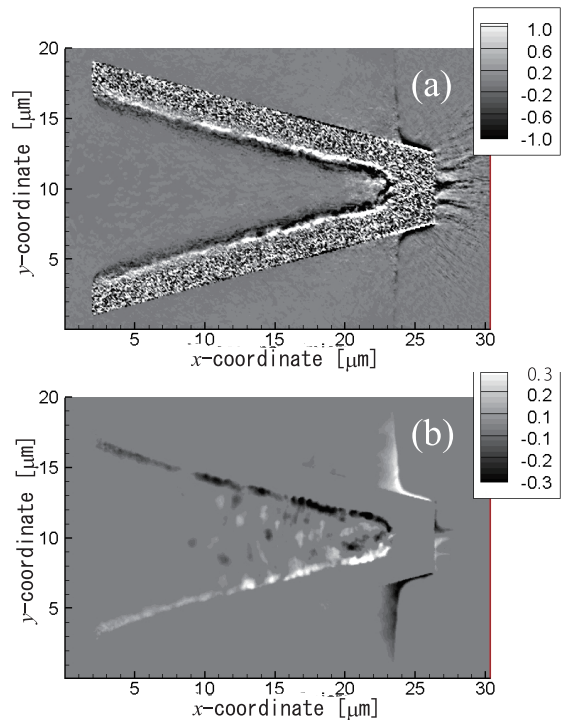


Fig. 2 (a) Distribution of the longitudinal current density which is normalized by  $-en_c$ . The surface current composed of high energy electrons is seen in black, which flows outside the critical surface, and the return current flows inside drawn in white. (b) The distribution of the static magnetic field which is normalized by the laser magnetic field is plotted. The magnitude of the laser magnetic field corresponds to 640 MG in this condition. The static magnetic field is localized along the target surface, which magnitude is up to 200 MG.

place, the effective temperature of high energy electrons becomes proportional to the laser spot size, i.e., lateral coordinate, which is not seen in the above simulation. This is because the acceleration length which is roughly  $10\mu\text{m}$  is relatively short for surface acceleration to play an important role, and the laser intensity is non-uniform along the surface due to the focal profile of laser energy and multiple reflections inside the target. For the larger cone target case, surface acceleration might play important role when the pre-plasma is pushed by the laser pressure to make a steep density front. In that case, the effective temperature will increase and might become higher than the ponderomotive energy of the incident laser pulses. The energy scalings for surface accelerated electrons will be discussed in another paper.

Another important feature of the cone target is that the laser field is amplified at the cone tip due to multiple reflections at the side wall. From a simple estimate assuming specular reflection, the laser light reflects 3 or 4 times inside the cone before it propagates backwards, where the number of reflections also depends on the ratio of the laser spot size and the tip diameter. Due to this multiple reflec-

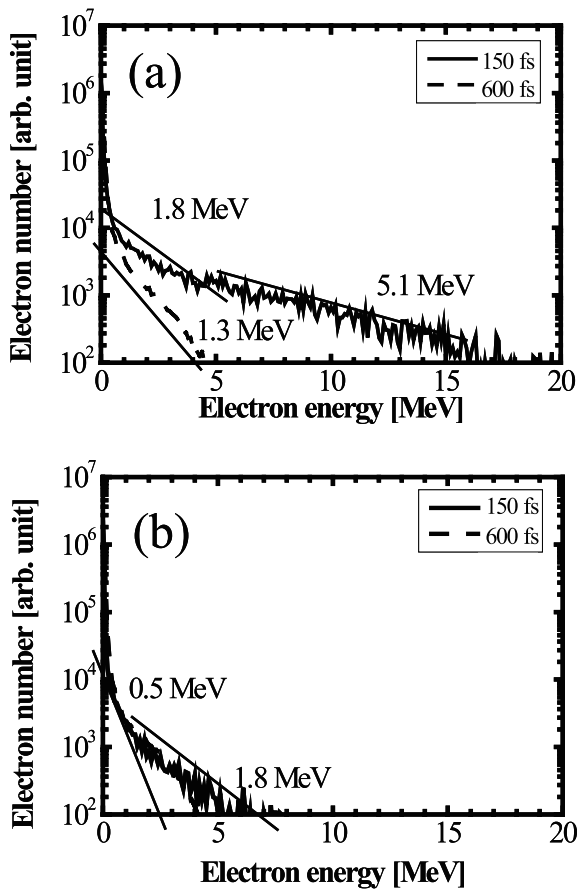


Fig. 3 Electron spectra observed at the cone tip plotted in (a), and the side wall plotted in (b). They are observed at  $x = 10$  and  $x = 24$ , respectively. High energy electrons accounting for  $T_{\text{hot}}$  are observed at the tip during the laser irradiation.

tion, the laser energy is focused at the cone tip increasing the laser irradiance. These intensified laser fields accelerate electrons ponderomotively, which characterize the electrons of the highest energy. In this simulation the laser field is intensified up to 4.2 times at the tip, which leads to a corresponding ponderomotive energy which is approximately equal to  $T_{\text{hot}}$ . This multiple reflection of laser fields also results in a higher energy absorption rate. In Fig. 3, the electron spectrum observed at the cone tip and side wall are plotted during the laser irradiation and after the irradiation. It is seen that high energy electrons with energy  $\geq 5.0$  MeV which are fitted by  $T_{\text{hot}}$  are observed during the irradiation at the tip and not at the side wall. This also confirms that the high energy electrons are accelerated at the cone tip by an intensified laser field. Since the laser intensification is controlled by the cone angle, characteristics of the highest energy electrons which are expressed by  $T_{\text{hot}}$  can be also controlled.

The above two acceleration processes taking place at the side wall and the tip are the dominant acceleration processes in the laser-cone interaction. Besides these processes electrons are accelerated at the target rear surface

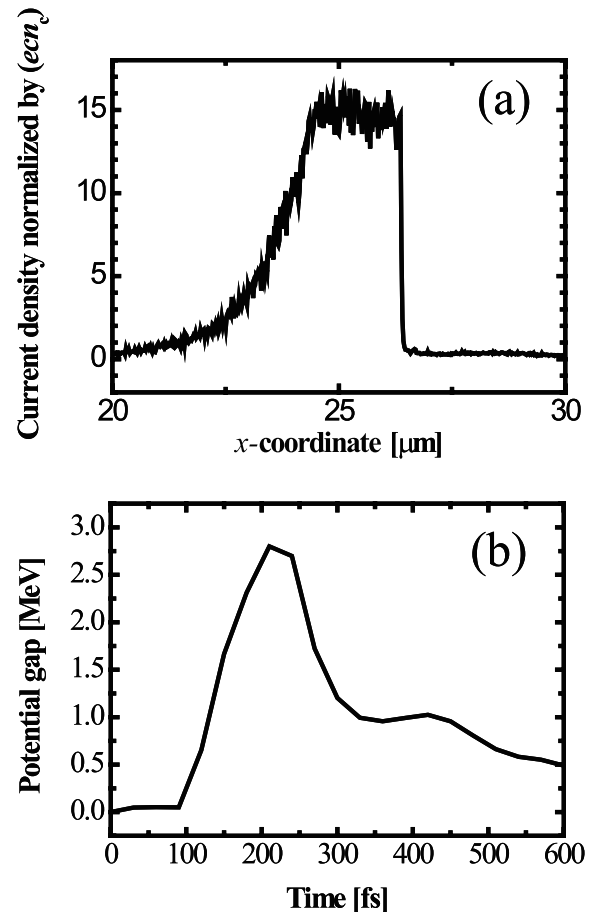


Fig. 4 (a) The forward current density around the cone axis is plotted at  $t = 210$  fs. The amount of current density is too high to be current-neutralized by the rear side plasma whose density is  $2 n_c$ . (b) Temporal change of the electrostatic field is induced at the rear surface. During the irradiation, the potential rises up to a few MeV, and drops after the irradiation is finished.

when a steep density gradient exists at the boundary of the cone and corona plasma [14]. In the above calculations we set the corona plasma at  $2 n_c$  which is smaller than the target density of  $100 n_c$ . The density distribution of forward current around the cone center axis is plotted in Fig. 4 (a) at  $t = 210$  fs. The return current flows in opposite direction which cancels out the forward current to achieve current-neutralization. But the forward current density at cone tip is too high to be neutralized by the rear side lower density plasma. As a result an electro-static field is induced at the rear surface, which is plotted in Fig. 4 (b). The potential gap increases during the laser irradiation (the laser pulse reaches the tip at about 80 fs and lasts for 150 fs) and decreases after the laser is off. The potential gap is up to a few MeV, which confines accelerated electrons inside the cone target reducing the outflow of the current density. At the same time, the static field accelerates cold electrons on the rear side towards the cone target, which account for  $T_{\text{low}}$ . Finally, we want to mention the angular distri-

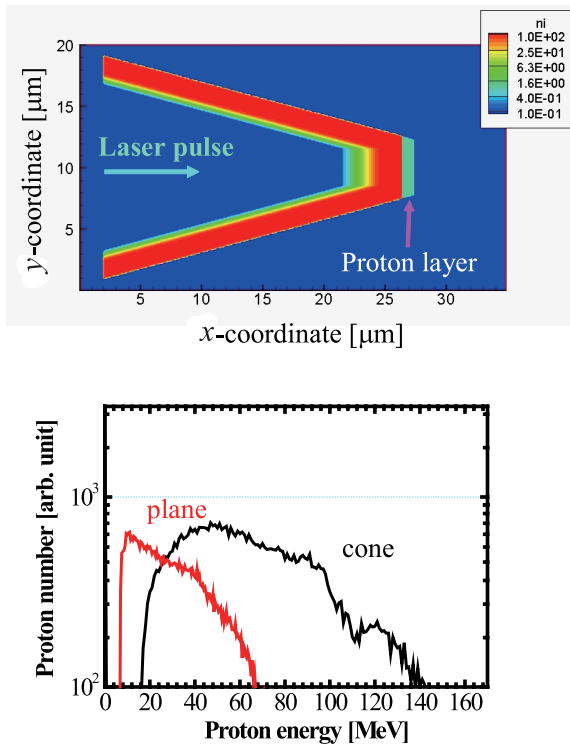


Fig. 5 (a) Initial profile of the cone target where a thin proton layer is attached in front of the target. (b) Comparison of the proton energy spectra accelerated by the cone and plane target.

bution of high energy electrons. The deviation the angle of electron propagation direction from laser axis is evaluated  $2.0\mu\text{m}$  behind the target. About 53% of the high energy electrons are within  $60^\circ$  and 29% are within  $30^\circ$ . This angular spread becomes smaller when the rear side plasma density becomes higher to reduce the density gap.

#### 4. Application to Proton Acceleration

One idea to utilize the advantage of cone targets of controlling the electron energy characteristics is proton acceleration by the laser-cone interaction. Proton acceleration by irradiating ultra-intense laser pulses onto solid targets has been studied intensively [15]. Increasing the proton maximum energy is one of the most important issues and target refinement such as ultra-thin targets [16], double layer targets [17] etc. have been proposed. Since the cone targets enhance the laser irradiance at the cone tip, it is expected to generate protons with higher energy than plane targets. We performed 2D PIC simulation for proton acceleration with the following conditions. The laser irradiance is  $4.0 \times 10^{20} \text{ W/cm}^2$  and pulse duration is 150 fs with a spot size of  $5\mu\text{m}$ . The cone and plane target have densities of  $100 n_c$ . A proton layer of  $1 n_c$  is attached at the rear surface to utilize the effect of the double-layer target, as is shown in Fig. 5 (a). Energy spectra of accelerated protons are shown in Fig. 5 (b). The maximum proton energy

from the cone target is about twice as large as that from the plane target. This is consistent with the results shown in Sec. 2, where the effective temperature of the hot electrons is two times higher for the cone target than for the plane target. This result shows the possibility to control proton energy via the laser-cone interaction by controlling the intensification of the laser energy at the cone tip.

#### 5. Summary and Conclusions

It is clarified that there are two electron acceleration processes which play an important role in the laser-cone interaction. One is electron acceleration and transport at the side wall via surface magnetic and electric fields. The second is the ponderomotive acceleration at the cone tip by the intensified laser pulse. These acceleration processes lead to the high energy electrons whose effective temperatures are modified from the ponderomotive energy of the irradiating laser pulse. Thus, it is possible to control the electron energy characteristics by controlling two acceleration processes which is done by optimizing the cone shape. As one example of the application of cone targets, proton acceleration using a double layer cone target is presented, which shows great enhancement of the proton maximum energy compared to the plane target. For the use in the fast ignition scheme, an abundant amount of electrons with energies of about  $1.0\text{MeV}$  is required. The understanding of the electron acceleration processes helps in the optimization of the cone target for fast ignition, which will be done in the near future.

#### Acknowledgments

This work is supported by MEXT, the Grant-in-aid for Creative Scientific Research (15GS0214) and partially the Grant-in-Aid for Encouragement of Young Scientists (B) (18740351).

- [1] S.P. Hatchett, C.G. Brown, T.E. Cowan, E.A. Henry, J.S. Johnson, M.H. Key, J.A. Koch, A.B. Langdon, B.F. Lasinski, R.W. Lee, A.J. Mackinnon, D.M. Pennington, M.D. Perry, T.W. Phillips, M. Roth, T.C. Sangster, M.S. Singh, R.A. Snavely, M.A. Stoyer, S.C. Wilks and K. Yasuike, *Phys. Plasmas* **7**, 2076 (2000).
- [2] T. Katsouleas, *Nature (London)* **431**, 515 (2004); and references therein.
- [3] J. Fuchs, Y. Sentoku, S. Karsch, J. Cobble, P. Audebert, A. Kemp, A. Nikroo, P. Antici, E. Brambrink, A. Blazevic, E.M. Campbell, J.C. Fernandez, J.C. Gauthier, M. Geissel, M. Hegelich, H. Pepin, H. Popescu, N. Renard-LeGalloudec, M. Roth, J. Schreiber, R. Stephens and T.E. Cowan, *Phys. Rev. Lett.* **94**, 045004 (2005).
- [4] M. Tabak, J. Hammer, M.E. Glinsky, W.L. Kruer, S.C. Wilks and R.J. Mason, *Phys. Plasmas* **1**, 1626 (1994).
- [5] R. Kodama, K. Shigemori, Y. Toyama, S. Fujioka, H. Azechi, H. Fujita, H. Habara, T. Hall, Y. Izawa, T. Jitsuno, Y. Kitagawa, K.M. Krushelnick, K.L. Lancaster, K. Mima, K. Nagai, H. Nishimura, T. Norimatsu, P.A.

- Norreys, S. Sakabe, K.A. Tanaka, A. Youssef, M. Zepf and T. Yamanaka, *Nature (London)* **418**, 933 (2002).
- [6] T. Johzaki, H. Nagatomo, H. Sakagami, T. Nakamura, K. Mima, Y. Nakao and T. Yokota, *Proceedings of Inertial Fusion Sciences and Applications 2005, Biarritz, to be published*; R.B. Campbell, R. Kodama, T.A. Melhorn, K.A. Tanaka and D.R. Welch, *Phys. Rev. Lett.* **94**, 055001 (2005).
- [7] R.B. Stephens, R.A. Snavely, Y. Aglitskiy, F. Amiranoff, C. Andersen, D. Batani, S.D. Baton, T. Cowan, R.R. Freeman, T. Hall, S.P. Hatchett, J.M. Hill, M.H. Key, J.A. King, J.A. Koch, M. Koenig, A.J. MacKinnon, K.L. Lancaster, E. Martinoli, P. Norreys, E. Perelli-Cippo, M. Rabec Le Gloahec, C. Rousseaux, J.J. Santos and F. Scianitti, *Phys. Rev. E* **69**, 066414 (2004).
- [8] Y. Sentoku, H. Ruhl, K. Mima, R. Kodama, K.A. Tanaka and Y. Kishimoto, *Phys. Plasmas* **6**, 2855 (1999).
- [9] R. Kodama, Y. Sentoku, Z.L. Chen, G.R. Kumar, S.P. Hatchett, Y. Toyama, T.E. Cowan, R.R. Freeman, J. Fuchs, Y. Izawa, M.H. Key, Y. Kitagawa, K. Kondo, T. Matsuoka, H. Nakamura, M. Nakatsutsumi, P.A. Norreys, T. Norimatsu, R.A. Snavely, R.B. Stephens, M. Tampo, K.A. Tanaka and T. Yabuuchi, *Nature (London)* **432**, 1005 (2004).
- [10] S.C. Wilks, W.L. Kruere, M. Tabak and A.B. Langdon, *Phys. Rev. Lett.* **69**, 1383 (1992).
- [11] T. Nakamura, S. Kato, H. Nagatomo and K. Mima, *Phys. Rev. Lett.* **93**, 265002 (2004).
- [12] M. Chen, Z.M. Sheng, J. Zheng, Y.Y. Ma, M.A. Bari, Y.T. Li and J. Zhang, *Opt. Express* **14**, 3093 (2006).
- [13] T. Nakamura, K. Mima, H. Sakagami and T. Johzaki, *Phys. Plasmas* **14** (2007) *to be published*.
- [14] H. Sakagami, T. Johzaki, H. Nagatomo and K. Mima, *Laser Part. Beams* **24**, 1 (2006).
- [15] E.L. Clark, K. Krushelnick, M. Zepf, F.N. Beg, M. Tatarakis, A. Machacek, M.I.K. Santala, I. Watts, P.A. Norreys and A.E. Dangor, *Phys. Rev. Lett.* **85**, 1654 (2000); R.A. Snavely, M.H. Key, S.P. Hatchett, T.E. Cowan, M. Roth, T.W. Phillips, M.A. Stoyer, E.A. Henry, T.C. Sangster, M.S. Singh, S.C. Wilks, A. MacKinnon, A. Offenberger, D.M. Pennington, K. Yasuike, A.B. Langdon, B.F. Lasinski, J. Johnson, M.D. Perry and E.M. Campbell, *Phys. Rev. Lett.* **85**, 2945 (2000).
- [16] M. Kaluza, J. Schreiber, M.I.K. Santala, G.D. Tatarakis, K. Eidmann, J. Meyer-ter-Vehn and K.J. Witte, *Phys. Rev. Lett.* **93**, 045003 (2004).
- [17] T. Esirkepov, K. Nishihara, S.V. Bulanov and F. Pegorano, *Phys. Rev. Lett.* **89**, 275002 (2002).